Sliding Mode Vector Control of Non-Sinusoidal Permanent Magnet Synchronous Machine

José Roberto B. A. Monteiro, Allan G. de Castro and Thales E. P. de Almeida
School of Engineering of São Carlos - EESC
University of São Paulo
São Carlos, SP 13566-590
Email: jrm@sc.usp.br

***Abstract*—This work presents a sliding mode controller for the speed control of a surface-mount permanent magnet synchronous machine (PMSM) with non-ideal trapezoidal back-EMF, using vectorial non-sinusoidal modeling. The calculus of vector-based machine model considers an ideal trapezoidal back-EMF waveform, i.e., all control calculation is based on ideal back-EMF, but they are applied to a machine with a real back-EMF waveform, which can be considered a distorted trapezoid. For the sliding controller, this paper shows the use of a sigmoidal function, the hyperbolic tangent, instead of the signal function and uses a proper sliding surface that presents combined integrative action and anti-windup effect, which is applied to the vector-based model of the non-sinusoidal machine. The final system consists in a high performance controller, robust to machine parameters and disturbances, and light in its design as shown by the results. The chosen sliding surface with integrative control action, combined to an anti-windup feature and the torque ripple free vector-based model, give zero steady state speed error, minimizes the system speed output overshoot and ripple.**

***Keywords*—sliding mode control, vector PMSM control, motor speed control, anti-windup.**

I. Introduction

Basically, surface-mount permanent magnet synchronous machines (PMSM) can be classified into two main categories, which is related to its back-EMF waveform: sinusoidal machines and trapezoidal machines. As expected, there are no absolute pure sinusoidal back-EMF waveforms and in the same way, there are not purely trapezoidal back-EMF waveforms. This work deals with trapezoidal machines, or better to say, non-sinusoidal back-EMF machines. This term is used to refer to a wide variety of back-EMF waveforms considered trapezoidal [1].

It is useful to make a note about the term brushless DC motor, which refers to the set composed by a non-sinusoidal (or trapezoidal) surface-mount permanent magnet synchronous machine and its electric power converter, commonly a three phase machine with a three phase electric converter (a three phase inverter) [2][1]. Considering an ideal trapezoidal back-EMF waveform and an equally ideal 120° square wave stator current, the machine produces an almost ripple free electromagnetic torque, as in Fig. 1. In this case the converter operates in six-step mode where each inverter bridge switch is active during 120° electrical, resulting in 2 switches on simultaneously. However, there are no machines with pure trapezoidal back-EMF waveforms and it is not possible to produce ideal 120° square-wave currents, resulting in electromagnetic torque ripple, and its values can be high, depending on the application [3].

Lately, in [4] is presented a vector control approach of the BLDC to reduce the torque ripple.

In this work the vector model based control of surface-mount permanent magnet synchronous machine with non-sinusoidal back-EMF is implemented considering second order sliding mode speed controller.

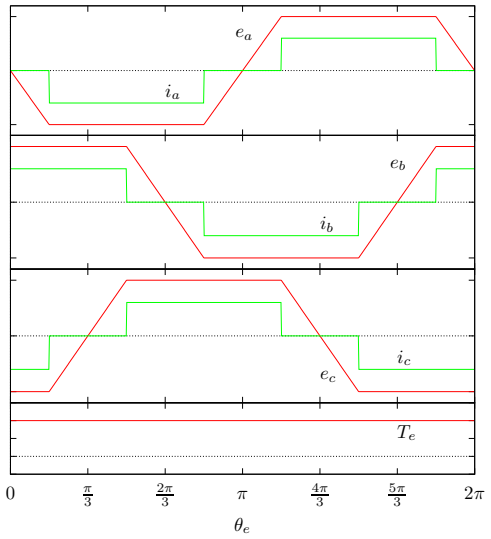

Fig. 1. Brushless DC motor ideal electromagnetic torque generation (θ_e: electrical position of the rotor).

II. Machine Modeling

The machine model is very studied in the literature and can be easily found, as in [4]. Just for better reference is shown here:

$$\begin{bmatrix} v_a \\ v_b \\ v_c \end{bmatrix} = \begin{bmatrix} L_s & M_s & M_s \\ M_s & L_s & M_s \\ M_s & M_s & L_s \end{bmatrix} \frac{d}{dt} \begin{bmatrix} i_a \\ i_b \\ i_c \end{bmatrix} + R_s \begin{bmatrix} i_a \\ i_b \\ i_c \end{bmatrix} + \begin{bmatrix} e_a \\ e_b \\ e_c \end{bmatrix} + \begin{bmatrix} v_n \\ v_n \\ v_n \end{bmatrix} \quad (1)$$

where:

e_a, e_b and e_c: induced voltage of stator phases a, b and c, respectively, due to rotor magnets movement, as in (2);
i_a, i_b and i_c: stator phase currents a, b and c, respectively;
L_s: stator phase self-inductance;
M_s: stator phases mutual inductances;
R_s: stator phase resistance;
v_a, v_b and v_c: a, b and c stator phases applied voltages, respectively;
v_n: stator neutral terminal voltage (this terminal is usually not connected).

Considering Φ_{ra}, Φ_{rb} and Φ_{rc} the linked magnetic fluxes between rotor magnets and stator winding phases a, b and c, respectively:

$$\begin{bmatrix} \Phi'_{ra} \\ \Phi'_{rb} \\ \Phi'_{rc} \end{bmatrix} = \frac{d}{d\theta_e} \begin{bmatrix} \Phi_{ra} \\ \Phi_{rb} \\ \Phi_{rc} \end{bmatrix} = \frac{1}{\omega_e} \begin{bmatrix} e_a \\ e_b \\ e_c \end{bmatrix} = \frac{1}{\omega_e} \frac{d}{dt} \begin{bmatrix} \Phi_{ra} \\ \Phi_{rb} \\ \Phi_{rc} \end{bmatrix} \tag{2}$$

where:

ω_e: electrical rotor speed.

$$T_{EL} = n_{pp} \left(\Phi'_{ra} i_a + \Phi'_{rb} i_b + \Phi'_{rc} i_c \right) \tag{3}$$

where:

T_{EL}: machine-generated electromagnetic torque;
n_{pp}: number of machine's pole pairs;

Since the magnets are mounted in rotor surface, inductance variation due to rotor position can be neglected [2].

The phases back-EMFs are ideally trapezoidal, therefore Φ'_{ra}, Φ'_{rb} and Φ'_{rc} are also trapezoidal as shown in Fig. 2, considering (2), where Φ_M is their amplitudes and θ_e is the rotor angle in electrical degrees.

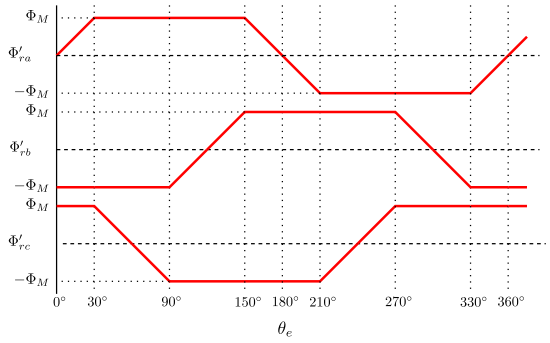

Fig. 2. Waveforms for Φ'_{ra}, Φ'_{rb} and Φ'_{rc}.

A. PMSM Vectorial Modeling

The vector-based model of this machine has the main objective to obtain the electromagnetic torque equation proportional to a stator current component, as in the vector-based model for sinusoidal machines. In order to achieve that, a special transformation is used additionally to the transformations used for the sinusoidal one, i.e., $\alpha\beta$ and dq transformations. This transformation is referred here by dq_x transformation [4] and is applied following to the dq one, as shown in Fig. 3 and is written as:

$$x_{\alpha\beta} = a_x e^{j\theta_x} e^{j\theta_e} x_{dq_x} \tag{4}$$

where:

a_x: dq_x size of axes, relatively to dq axes, which are considered equal to the unity;
θ_x: angle of dq_x axes , relatively to dq axes.

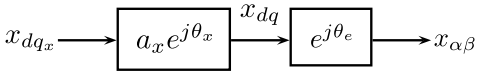

Fig. 3. dq_x transformation represented by blocks.

The $\alpha\beta$ transformation is:

$$x_{\alpha\beta} = \sqrt{\frac{2}{3}} \begin{bmatrix} 1 & e^{j\frac{2\pi}{3}} & e^{-j\frac{2\pi}{3}} \end{bmatrix} \begin{bmatrix} x_a \\ x_b \\ x_c \end{bmatrix} \tag{5}$$

$$x_0 = \sqrt{\frac{2}{3}} \begin{bmatrix} \frac{\sqrt{2}}{2} & \frac{\sqrt{2}}{2} & \frac{\sqrt{2}}{2} \end{bmatrix} \begin{bmatrix} x_a \\ x_b \\ x_c \end{bmatrix} \tag{6}$$

where:

$x_{\alpha\beta}$: quantities written over $\alpha\beta$ axes (complex number);
x_0: zero component;
x_a, x_b and x_c: quantities of a, b and c phases, respectively.

Applying those transformations to machine electric and torque equations, (1) and (3), and choosing a_x and θ_x as:

$$a_x = \sqrt{\frac{3}{2}} \frac{\Phi_m}{\sqrt{\Phi'^2_{r\alpha} + \Phi'^2_{r\beta}}} \tag{7}$$

$$\theta_x = \tan^{-1} \frac{-\Phi'_{r\alpha}}{\Phi'_{r\beta}} - \theta_e \tag{8}$$

The electromagnetic torque equation in dq_x axes is:

$$T_{EL} = n_{pp} \sqrt{\frac{3}{2}} \Phi_m i_{q_x} \tag{9}$$

And the electric equations:

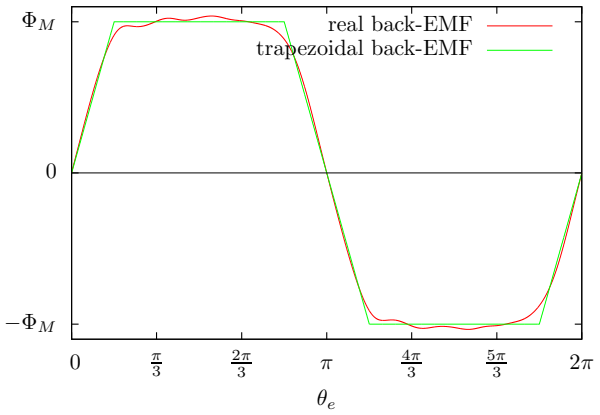

Fig. 4. Ideal trapezoidal back-EMF and measured back-EMF, of the real machine, waveforms.

$$v_{d_x} = R_s i_{d_x} + (L_s - M_s)\frac{di_{d_x}}{dt} + (L_s - M_s)\,\omega_e \left(i_{d_x}\frac{a_x'}{a_x} - i_{q_x}\left(1 + \theta_x'\right)\right)$$

$$v_{q_x} = R_s i_{q_x} + (L_s - M_s)\frac{di_{q_x}}{dt} + (L_s - M_s)\,\omega_e \left(i_{q_x}\frac{a_x'}{a_x} + i_{d_x}\left(1 + \theta_x'\right)\right) + \sqrt{\frac{3}{2}}\Phi_m \frac{1}{a_x^2}\omega_e \tag{10}$$

where:

$$a_x = \sqrt{\frac{3}{2}}\frac{\Phi_m}{\sqrt{\Phi_{r\alpha}'^2 + \Phi_{r\beta}'^2}} \tag{11}$$

$$\theta_x = \tan^{-1}\frac{-\Phi_{r\alpha}'}{\Phi_{r\beta}'} - \theta_r \tag{12}$$

The measured back-EMF waveform for one phase together with an ideal trapezoidal back-EMF waveform are shown in Fig. 4. The coefficients for those back-EMF waveforms are shown in Figs. 5 and 6, for a_x and θ_x respectively. For the vector control, the coefficients for the trapezoidal back-EMF are used, but the machine model employs the real back-EMF waveform. This causes a difference in dq_x currents, but with minimal influence on electromagnetic torque, as seen in Sec. IV.

III. Sliding Mode Control

A block diagram of the complete drive system is shown in Fig. 7, where there are three controllers: the stator current controllers, C_{d_x} and C_{q_x}, for direct and quadrature controllers; and the rotor speed controller, C_ω. As the time constant of mechanical system is far greater than the time constant of electrical system, rotor speed control loop are weakly coupled to current control loops, which are strongly coupled to one another. Thus, it is possible to make separate analysis for the controllers of speed loop (C_ω) and for current loops (C_{d_x} and C_{q_x}) [5].

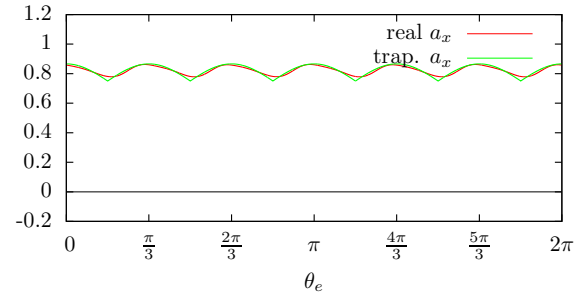

Fig. 5. Coefficient a_x for the measured back-EMF of the real machine and for an ideal trapezoidal back-EMF.

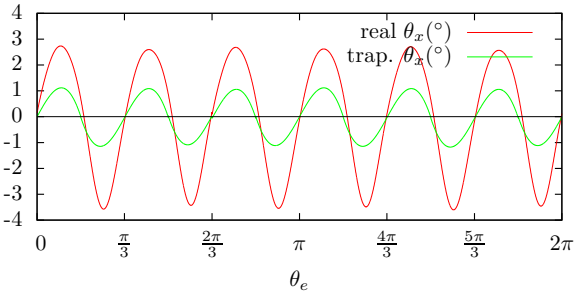

Fig. 6. Coefficient θ_x for the measured back-EMF of the real machine and for an ideal trapezoidal back-EMF.

The current controllers are first order sliding mode controllers, as in [6], so their sliding mode variables are:

$$\begin{aligned}\sigma_{d_x} &= i_{d_x}^* - i_{d_x}\\ \sigma_{q_x} &= i_{q_x}^* - i_{q_x}\end{aligned} \tag{13}$$

where

$i_{d_x}^*$: stator line direct axis current reference,
$i_{q_x}^*$: stator line quadrature axis current reference,
i_{d_x}: stator line current for direct axis, and
i_{q_x}: for quadrature axis.

And the stator current controller is:

$$\begin{aligned}C_{d_x}: &\quad v_{d_x} = \tanh k_I \cdot \sigma_{d_x}\\ C_{q_x}: &\quad v_{q_x} = \tanh k_I \cdot \sigma_{q_x}\end{aligned} \tag{14}$$

The reachability and the sliding mode conditions of the current controller for the first order sliding mode controller (14) are both shown in [6].

A. Rotor Speed Sliding Mode Controller

The used sliding variable for the speed control loop is [7]:

$$\sigma = \int \left(\lambda(\epsilon) + \frac{d}{dt}\right)^{r-1} \epsilon\, dt \tag{15}$$

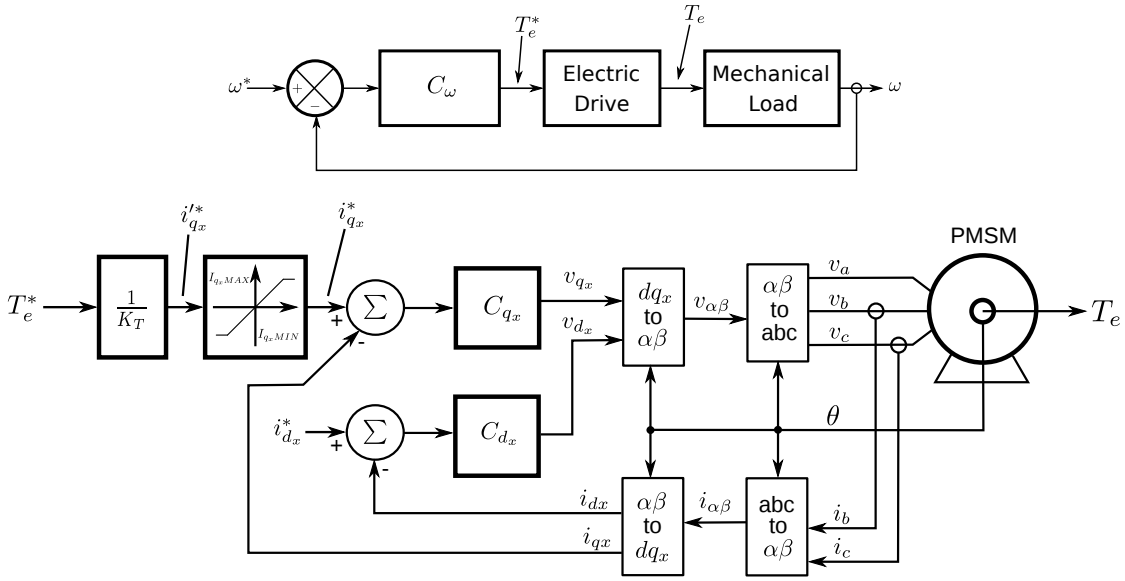

Fig. 7. System complete control block diagram ($K_T = 2n_{pp}\Phi_M$, C_ω: rotor speed controller, C_{d_x}: stator direct current controller, C_{q_x}: stator quadrature current controller).

where:

$\epsilon = x^* - x$;
r: is the degree of sliding surface;
x: vector of state variables;
x^*: references for state variables;

The sliding surface is defined as $\sigma = 0$ and one must note that it differs from the commonly generic sliding variable shown in [8].

Due to the use of the integral operator, λ must be a function of $x^* - x$. For this application, it is considered a sliding surface of order 2 ($r = 2$). The function λ must be chosen according to the application in order to satisfy the reachability and attractability criteria. Therefore, the speed loop controller is a sliding mode of order 2, and its sliding surface is:

$$\sigma_\omega = \int \lambda(\epsilon_\omega)\epsilon_\omega dt + \epsilon_\omega = 0 \tag{16}$$

where:

σ_ω: sliding variable for rotor speed control loop (C_ω);
$\epsilon_\omega = \omega^* - \omega$: shaft speed error;
ω^*: rotor speed reference;
ω: measured rotor speed.

The dynamic mechanical load equation is:

$$\frac{d\omega}{dt} = \dot{\omega} = -\frac{B}{J}\omega - \frac{1}{J}T_L + \frac{1}{J}T_{EL} \tag{17}$$

where:

B: equivalent frictional coefficient, composed by rotor shaft bearings and load frictional losses;
J: combined inertia momentum of machine rotor and load;
T_L: load torque;

B. System convergence

A general non-linear system can be written as:

$$\begin{aligned} \dot{x} &= f(x) + g(x)U \\ y &= h(x) \end{aligned} \tag{18}$$

where:

U: system input;
f, g, h: linear or non-linear functions, characterizing the system;
y: system output.

The system input function U can be written as a sum of a continuous function and a switching function:

$$U = U_{eq} + U_c \tag{19}$$

where:

U_{eq}: is a continuous function and is referred as "equivalent control", representing the operation point where the sliding regime occurs [9];
U_c: is the switching control, representing the variable structure of the system, responsible to the attractiveness of the system to the sliding regime.

A well accepted method to prove the convergence of that system to the operation point is by the definition of an energy Lyapunov function and giving the conditions to be satisfied, the final inequality is [7]:

$$\frac{\partial \sigma}{\partial x} g(x) < 0 \ \text{ for } \ \sigma \neq 0 \tag{20}$$

The use of a sigmoidal function does not alter the inequality (20) as well.

In order to prove the sliding mode of the system, the equivalent control must conform to systems limits and in order to prove the reachability condition, so (20) must be satisfied. Using (17), the equivalent control of the system input (T_{EL}) is:

$$T_{EL_{eq}} = B\omega + T_L \tag{21}$$

Considering the bounding limits of operation, in the maximum desired speed, maximum machine electromagnetic torque must equals the product of maximum speed and shaft friction coefficient plus maximum load torque.

In order to prove that the system stays in the adopted sliding surface, considering $g(x) = 1/J$ in (16), (20) leads to:

$$\frac{\lambda(\epsilon_\omega)\epsilon_\omega}{\dot{\omega}} - 1 < 0 \Rightarrow \frac{\lambda(\epsilon_\omega)\epsilon_\omega}{\dot{\omega}} < 1 \Rightarrow \tag{22}$$

$$\lambda(\epsilon_\omega) < \frac{\dot{\omega}}{\epsilon_\omega} \tag{23}$$

Using: $\dot{\omega} = -\frac{B}{J}\omega - \frac{1}{J}T_L + \frac{1}{J}T_{EL} = \frac{B}{J}\epsilon_\omega - \frac{1}{J}T_L - \frac{B}{J}\omega^* + \frac{1}{J}T_{EL}$ and considering limit operational values for T_L and i, which gives maximum allowed T_{EL}:

$$\lambda(\epsilon_\omega) < \frac{B}{J} + \frac{\frac{1}{J}(T_{EL} - T_L)}{\epsilon_\omega} - \frac{\frac{B}{J}\omega^*}{\epsilon_\omega} \tag{24}$$

That results in a hyperbole depending on ω^*. When $\epsilon_\omega < 0$, $T_{EL} < 0$ and considering T_{EL} the preponderant factor of the equation, then the hyperbole is always positive. So $\lambda(\epsilon_\omega)$ must be inscribed in that hyperbole in order to satisfy the reachability condition (Fig.8).

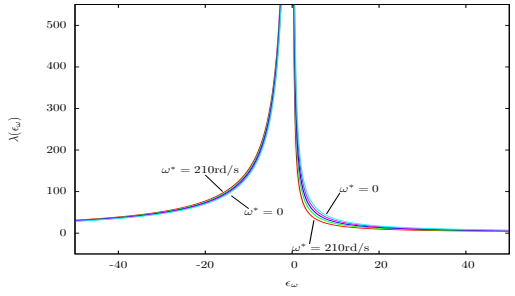

Fig. 8. Hyperbole delimiting reachability condition.

IV. Results

The used machine and its load has the parameters shown in Table I. The load torque (T_L) is 2.2Nm for this machine.

Simulation results are shown in Figs. 9 to 10. In the figures, the load torque is varied abruptly from 0 to its maximum value (2.2Nm) and to its maximum in the opposite direction (-2.2Nm). Fig. 9 shows the machine accelerating and reaching 1000rpm of rotor speed. The details of machine speed is shown in Fig. 10, where it decreases when torque load increases and *vice-versa*.

TABLE I. BLDC motor and mechanical load parameters used in simulations.

Motor	Load
$R_s = 2.3\Omega$	$J = 4.2 \cdot 10^{-3}$kg m^2
$(L_s - M_s) = 12.5$mH	$B = 3.032 \cdot 10^{-3}$kg m^2/s
$n_{pp} = 3$	
$\Phi_m = 0.12$Wb	

Fig. 11 shows details of electromagnetic torque and its reference for the quadrature current component. It can be seen that produced torque is almost free of ripple, even considering a different back-EMF waveform, as the coefficients a_x and θ_x where evaluated using a pure trapezoidal waveform, which is different from that of the machine under test.

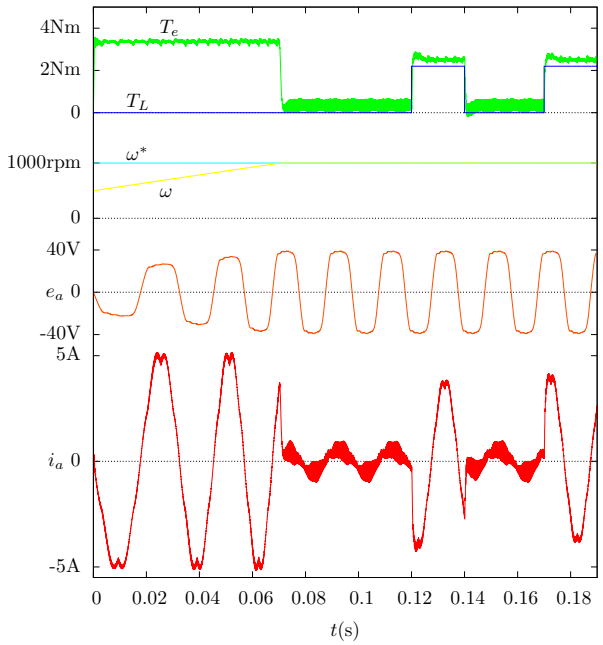

Fig. 9. Machine operation at 1000rpm, with control using a_x and θ_x coefficients evaluated for an ideal trapezoidal back-EMF waveform but applied in a real back-EMF machine used.

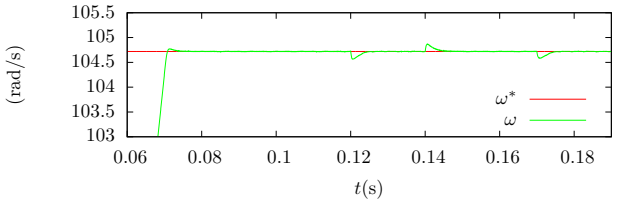

Fig. 10. Machine operation at 1000rpm, detail of speed during load torque transients.

Fig. 12 shows the machine accelerating from 1000rpm and reaching 2000rpm. During this interval, load torque is

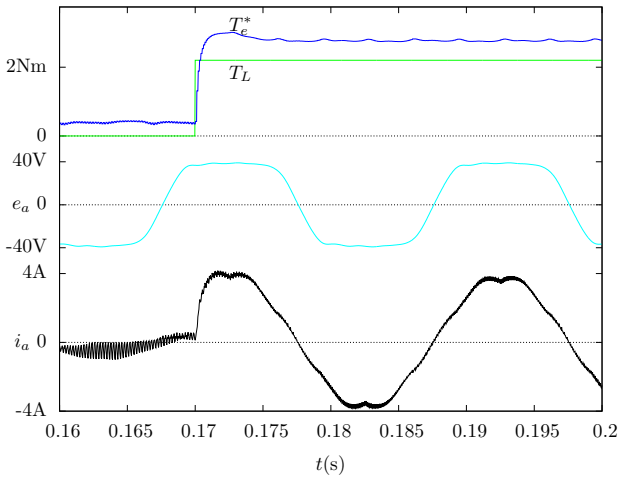

Fig. 11. Machine operation at 1000rpm, detail of reference torque chattering.

applied against machine motion (positive value) and favoring its motion (negative value). Those load torque changes causes some transients in machine speed. After machine achieves its set point speed, it occurs a little overshoot due to load torque favoring its motion (Fig. 13). In $t = 0.35$s, load torque is released, so machine speed falls but integrative action of the controller put it back to its set point. In $t = 0.4$s, a load torque against its motion is applied, so machine speed falls again, but due to integrative action, it reaches its set point after 50ms. When this load is released, machine accelerates but it is back to its set point again.

V. Conclusions

Considering the results, the ripple in speed is practically nonexistent due to almost absence of torque ripple, even considering an ideal trapezoidal back-EMF for the controller and a real back-EMF (distorted trapezoidal waveform) for the machine. As the back-EMF waveform of the machine has minor variation in its normal region of operation, the control presents a good performance.

This work combines a sliding surface and non-sinusoidal vector-based model in order to minimize electromagnetic torque ripple and eliminate the steady state error of the system which is introduced by the use of analog functions as switching functions, instead of the signal function. The use of an analog function, as the hyperbolic tangent function, can reduce significantly system chattering, but it is not properly a sliding mode control and causes non-zero steady state error, as pointed out by the literature. The anti-windup effect achieved by the proposed surface is similar to the conventional method called conditional integration, but with the difference that the integrative portion is gradually activated as the error decreases, so the integrator is active even for large error values. This is a good feature once the conventional method can fail if the error does not fall into a range.

The combination of the vector-based model plus the sliding mode control shows excellent results for the control of machine rotor speed, i. e., fast speed response, no steady state error, minimum rotor speed overshoot, low torque ripple and no chattering.

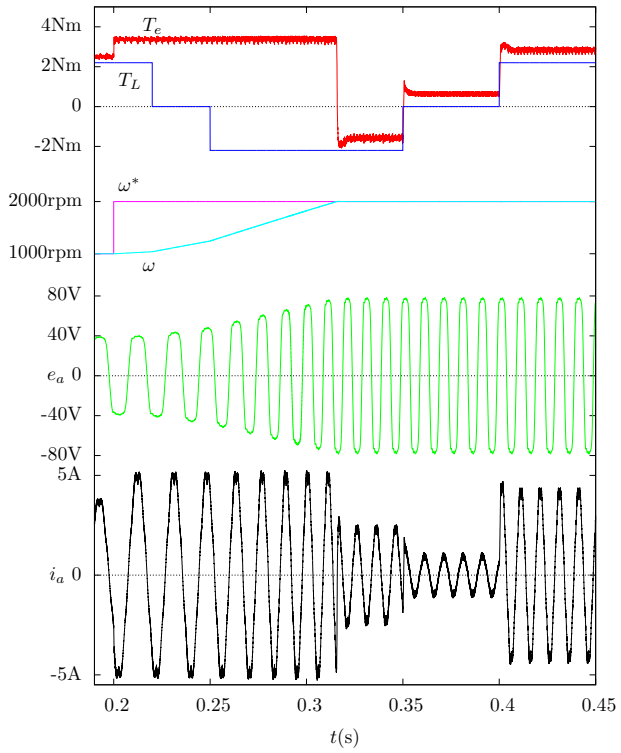

Fig. 12. Machine operation at 2000rpm, with control using a_x and θ_x coefficients evaluated for an ideal trapezoidal back-EMF waveform but applied in a real back-EMF machine used.

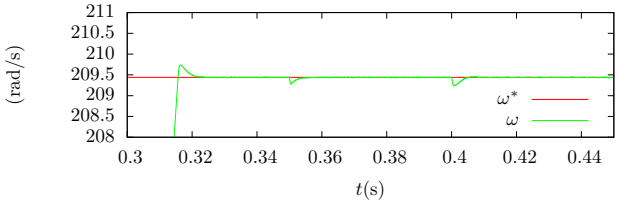

Fig. 13. Machine operation at 2000rpm, detail of speed during load torque transients.

Acknowledgments

The authors would like to acknowledge the grant #2006/04226-0, São Paulo Research Foundation (FAPESP).

References

[1] T. J. E. Miller, *Bushless Permanent-Magnet and Reluctance Motor Drives*. Oxford: Claredon Press, 1993.

[2] S. A. Nasar, I. Boldea, and L. E. Unnewehr, *Permanent magnet, reluctance, and self synchronous motors*. Boca Raton: CRC Press, 1993.

[3] J. Holtz and L. Springob, "Identification and compensation of torque ripple in high precision permanent magnet motor drives," *IEEE Transactions on Industrial Electronics*, vol. 43, no. 2, 1996.

[4] J. R. B. A. Monteiro, A. A. Oliveira, M. L. Aguiar, and E. R. Sanagiotti, "Electromagnetic torque ripple and copper losses reduction in permanent magnet synchronous machines," *European Transactions on Electrical Power*, vol. 22, no. 5, pp. 627–644, June 2012, doi: 10.1002/etep.594.

[5] B. M. Patre, V. M. Panchade, and R. M. Nagarale, *Sliding Mode Control*. InTech, 2011, ch. Sliding Mode Control of DC Drives, available from: http://www.intechopen.com/books/sliding-mode-control/sliding-mode-control-of-dc-drives.

[6] C. M. R. Oliveira, J. R. B. A. Monteiro, and M. L. Aguiar, "Sliding mode control of brushless dc motor speed with chattering reduction," in *Proceedings of the 2015 IEEE 24th International Symposium on Industrial Electronics (ISIE)*. Búzios, Brazil: IEEE, June 2015, pp. 590–595.

[7] J. R. B. A. Monteiro, C. M. R. Oliveira, T. E. P. Almeida, and M. J. Cezare, "Pseudo sliding mode control with integrative action applied to brushless dc motor speed control," in *2015 IEEE 13th Brazilian Power Electronics Conference and 1st Southern Power Electronics Conference (COBEP/SPEC)*, Nov 2015, pp. 1–6.

[8] J. Slotine and W. Li, *Applied nonlinear control*. Englewood Cliffs: Prentice Hall, 1991.

[9] M. Mahmoudi, N. Madani, M. Benkhoris, and F. Boudjema, "Cascade sliding mode control of a field oriented induction machine drive," *The European Physical Journal Applied Physics*, vol. 7, pp. 217–225, 1999.